Sho, K., & Kondo, Y. (1984) *Biochem. Biophys. Res. Commun. 118*, 385-391.
Sugawara, M., Kita, T., Lee, E. D., Takamatsu, J., Hagen, G. A., Kuma, K., & Medeiros-Neto, G. A. (1988) *J. Clin. Endocrinol. Metab. 67*, 1156-1161.
Takasu, N., Yamada, T., & Shimizu, Y. (1987) *Biochem. Biophys. Res. Commun. 148*, 1527-1532.
Takeda, A., & Samejima, T. (1977) *Biochim. Biophys. Acta 481*, 420-430.
Tanaka, T., Makino, R., Iizuka, T., Ishimura, Y., & Kanegasaki, S. (1988) *J. Biol. Chem. 263*, 13670-13676.
Ueno, I., Kohno, M., Mitsuta, K., Mizuta, Y., & Kanegasaki, S. (1989) *J. Biochem. (Tokyo) 105*, 905-910.
Verma, S., Kumar, G. P., Laloraya, M., Singh, A., Nivsarkar, M., & Bharti, S. (1990) *Biochem. Biophys. Res. Commun. 169*, 1-7.
Yokota, K., & Yamazaki, I. (1977) *Biochemistry 16*, 1913-1920.

Investigation of Laser-Induced Long-Lived States of Photolyzed MbCO†

V. Šrajer, L. Reinisch, and P. M. Champion*
Department of Physics, Northeastern University, Boston, Massachusetts 02115
Received December 5, 1990; Revised Manuscript Received February 20, 1991

ABSTRACT: We present evidence from resonance Raman and absorption measurements that the extended exposure of MbCO to CW laser light at low temperatures alters the CO rebinding kinetics and leads to a significantly increased population of very long lived states of photolyzed MbCO. This optical "pumping" process is observed for samples frozen in both aqueous buffer and glycerol/buffer and exhibits power law behavior with a very weak temperature dependence. A comparison of the nonexponential rebinding kinetics of CO molecules from the pumped states with the rebinding observed in flash photolysis experiments suggests that the pumped states are distinct geminate states, not observed in flash photolysis experiments. Thus, a four-state model, with two geminate states, is implicated for MbCO. Pumped states may represent "separated geminate pair" states with the CO molecule still in the heme pocket or possibly trapped within a cavity on its way through the protein matrix, consistent with molecular dynamics simulations. The possibility of significant deoxyheme relaxation from a less domed to a more domed configuration, as a result of the multiple photolysis events associated with the pumping process, is also explored. However, the small changes observed in the Soret band line shape and position subsequent to pumping at $T < 180$ K tend to rule out this explanation for the pumping process. Since the yield for creating a pumped state is small (e.g., $<10^{-7}$ for $T > 100$ K), pumping can be observed only after extended illumination and is absent in flash photolysis measurements, even after multiple flashes. At higher temperatures ($T > 180$ K), the escape of the CO molecule to the solvent is observed. Our data are consistent with a "phase transition" of the protein that is coupled to the surrounding matrix. The protein fluctuations are quenched below ~185 K for a solvent composed of 70% glycerol and below ~260 K for aqueous buffer. We also present the first large amplitude measurements of CO rebinding from the protein exterior, observed below 200 K after freezing the sample under laser illumination.

MbCO at low temperatures has been extensively studied by use of the flash photolysis technique (Austin et al., 1975; Beece et al., 1980). These studies have revealed a nonexponential nature of the geminate rebinding process at low temperatures and require a distribution of exponential rebinding rates in order to be explained. Two possible scenarios for the observed power law rebinding are (1) all Mb molecules are identical and each has multiple sites with different rebinding rates (homogeneous ensemble) and (2) each molecule at low temperatures is frozen in a slightly different conformation than the other molecules (quenched disorder), leading to a distribution of rebinding rates throughout the ensemble (inhomogeneous ensemble). One experiment that can distinguish between these two possibilities involves photodissociating flashes that are repeated at time intervals short enough so that only partial rebinding occurs between two flashes. If all the molecules are identical and have a variety of sites for the photolyzed CO molecule to go to, repetitive flashes would lead to an increasing number of molecules with CO "trapped" at sites with smaller rebinding rates. Each flash will, thus, alter the distribution of rates and after each flash, slower rebinding would be observed. If, on the other hand, the ensemble of molecules is inhomogeneous, repetitive flashes will not alter the distribution of rates and, after each flash, the same nonexponential relaxation function will be observed. Since the multiple-flash experiment (Austin et al., 1975) in MbCO revealed no change in the rebinding after repeated pulses, it was concluded that inhomogeneity of the ensemble of Mb molecules was the source of the nonexponential rebinding behavior at low temperatures. The inhomogeneous distribution of protein conformations has been supported by several other measurements (Frauenfelder et al., 1979; Champion & Sievers, 1980; Parak et al., 1982; Hartmann et al., 1982) and model calculations (Case & Karplus, 1979) on Mb and Hb.

However, EXAFS experiments (Powers et al., 1984; Chance et al., 1986) showed that, after extended continuous illumination of a MbCO sample with white light, some pumping to long-lived states of photolyzed molecules occurs. Subsequent flash photolysis experiments (Ansari et al., 1987), performed

† This work is supported by Grant DMB8716382 from the NSF and Grant AM 35090 from the NIH.

0006-2960/91/0430-4886$02.50/0

before and after extended illumination with white light, confirmed the observation of an altered distribution of rates. The flash photolysis experiments also showed that the rebinding remained nonexponential, contradicting the exponential rebinding kinetics from pumped states reported in the EXAFS experiments.

The absence of the pumping effect in flash photolysis experiments, even after multiple flashes, suggests a low yield of the pumping process. Since the deoxy population can be followed only over a limited dynamic range in the flash photolysis measurements (seldom better than three decades), events with a low yield ($<10^{-4}$), which deplete the total geminate population by a small fraction, will go undetected. In the CW laser experiments, on the other hand, the system is constantly being cycled and many more "attempts" for ligand escape and heme relaxation are possible. This leads to the observation of a slow increase in the deoxy population with time rather than the rapid approach to equilibrium that is expected.

To better probe the characteristics of the pumping process and the nature of the pumped states, we have taken advantage of the very high photolysis rate associated with laser sources (10^3–10^4 s^{-1} for MbCO) and present a variety of experiments where the sample was illuminated for an extended time period ($\sim$1 h) with CW laser light at 425 nm. We have monitored the "pumping" of MbCO at various temperatures and laser powers under a variety of solvent conditions. We have also monitored the rebinding from the pumped states as a function of temperature and made comparisons to low-temperature flash photolysis measurements and rebinding from the protein exterior (using MbCO samples prepared with laser illumination during the freezing process).

Experimental Procedures

Lyophilized sperm whale metMb was obtained from Sigma Chemical Co. and U.S. Biochemical Corp. and was used without further purification. The protein was dissolved in an aqueous buffer (0.1 M potassium phosphate buffer) or aqueous buffer/glycerol mixture (75, 50, or 25% glycerol by volume was used) and equilibrated with 1 atm of CO. The protein was reduced with an excess of sodium dithionite dissolved in N_2 equilibrated water. The reduced solution was again equilibrated with CO. Glycerol/buffer solutions were equilibrated for $\sim$1–2 h. The final protein concentrations were $\sim$10 μM for absorption measurements and $\sim$1 mM for Raman measurements. The concentration was measured by using a Perkin Elmer UV–visible spectrophotometer (model 320).

The sample was placed in a low-temperature sample holder made from OFHC copper and electroplated gold. The optical window was a thin microscope cover slip for the Raman cell or two 1.5-mm-thick quartz windows for the transmission cell for absorption measurements. The sample holder was tightly screwed to the cold finger of an CTI Cryogenics Model 22C closed cycle refrigerator. An indium gasket and a thin film of Apiezon N grease was used to assure a good thermal contact between the cold finger and the sample holder. The temperature was monitored with a cryodiode mounted on the cold finger. Comparisons between readings of a diode mounted on the cold finger and one mounted in contact with the solution showed less than 1 K temperature difference between the sample and the cold finger over the entire temperature range (10–290 K).

The temperature was stabilized with a TRI Research T-2000 cryo controller unit to $\pm$0.2 K. The sample was allowed to equilibrate thermally for $\sim$20 min at any given temperature before it was illuminated with laser light. The samples were cycled through freezing and thawing several times with no measurable sample degradation noted.

The resonance Raman data were accumulated with a Spex Triplemate monochromator or Spex single monochromator, both equipped with 2400 g/mm gratings, and a Princeton Instruments optical multichannel analyzer (OMA). The absorption spectra were collected with the Spex single monochromator with a 300 g/mm grating and a Princeton Instruments OMA.

Three types of experimental procedures were performed. In procedure I, the sample was cooled to a given temperature and then illuminated for $\sim$1 h with 425 nm (23 529.5 cm^{-1}) CW laser light (5–10-mW typical power, 0.1-mm beam diameter). During the illumination $\sim$30 resonance Raman spectra were recorded. From the oxidation marker band region of the Raman spectra, the photolyzed and bound populations were monitored as a function of illumination time for processes slower than $\sim$1 s. We will refer to this procedure as preparation of a pumped state or simply pumping. The pumping of MbCO was studied for samples frozen in both aqueous buffer and glycerol/buffer mixtures.

In procedure II, the sample was cooled to a given temperature and then illuminated with CW laser light for $\sim$1 h so that pumped states were prepared. The laser light was turned off and the absorption line shapes in the Soret region were monitored with a weak (photolysis rate $\sim 10^{-3}$ s^{-1}) white light probe, filtered through $\sim$2-cm-thick heat-absorbing glass. We found that the spectra were fully explained by a superposition of the deoxy Mb* and MbCO Soret bands, thus confirming that no photochemistry was taking place during the pumping process. The populations of photolyzed and bound species were then monitored during rebinding from the pumped state for processes slower than 1 min. To assure that the same, previously illuminated region of the sample was interrogated, two pinholes ($\sim$0.5 mm in diameter, placed before and after the sample) were used. Both light beams (the laser during the pumping phase and the white light during the rebinding phase) were aligned to pass through and fill the pinholes. The typical laser power used in the pumping phase in this procedure was 30 mW at 425 nm. The rebinding from the pumped state was studied only for 75% glycerol samples since they have a clear, glassy appearance (except for several cracks) when frozen and allow the absorption measurement. During the pumping phase in procedures I and II, the stability of the laser power was monitored and runs with a change in power larger than 10% were discarded.

In procedure III, the MbCO sample was cooled from room temperature to a low temperature (160–200 K) by using CW laser light illumination (power $\sim$30 mW) to keep the sample in the photolyzed state. The laser light was then blocked, and rebinding was monitored with a weak white light probe beam in the Soret absorption region. As in procedure II, two pinholes were used and processes slower than 1 min were monitored in solutions containing 75 and 50% glycerol.

The CW laser light was generated by a Coherent CR-699 dye laser with Stilbene 3 dye, pumped with a Coherent Innova 100 argon ion laser. The white probe light in the CO-rebinding measurements was generated by a quartzline GE 100-W lamp.

Results

The effect of extended exposure of MbCO to CW laser light at low temperatures, as monitored by the resonance Raman technique (procedure I), is presented in Figure 1. The oxidation marker band region (ν_4) is shown with the 1356-cm^{-1} mode of photolyzed Mb and the 1372-cm^{-1} mode of MbCO. It can be seen that a photostationary equilibrium is not reached

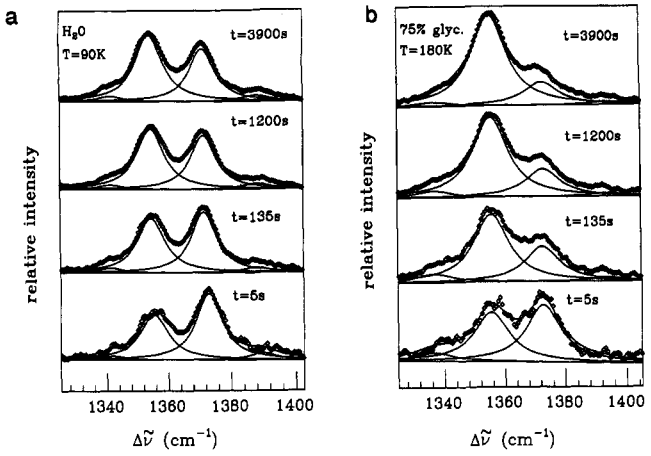

FIGURE 1: The effect of extended exposure of MbCO to 5-mW CW laser light ($J_l \simeq 1.2 \times 10^{20}$ photons/(cm^2 s)) at 425 nm ($k_l = J_l\sigma_A$(425 nm) = 7.0×10^4 s^{-1}) monitored by the resonance Raman technique. The oxidation marker band region (ν_4) is shown with the 1356-cm^{-1} mode of photolyzed species and the 1373-cm^{-1} mode of CO-bound species. The data show that a steady state has not been reached even after more than 1 h of laser illumination of the sample. Instead, the population of photolyzed species continuously increases during the illumination. This "pumping" effect is present in both aqueous buffer (a) and glycerol/buffer (b) solutions.

even after more than an hour of illumination with 5 mW of 425-nm CW laser light. For a two-state system, it is expected that steady state is reached in $\tau_{eq} = (k_l + \langle k_{BA}\rangle)^{-1}$, where k_l is the photon-induced photolysis rate per molecule and $\langle k_{BA}\rangle$ is the average geminate rebinding rate. The estimated value for k_l in our experiment is of the order of 10^3–10^4 s^{-1}, which sets an upper limit on the "equilibration time": $\tau_{eq} < 1$ ms. However, a significant increase in the photolyzed Mb population is observed on the time scale of minutes and hours. This pumping process is present in both aqueous buffer (Figure 1a) and glycerol/buffer samples (Figure 1b). The biggest increase in photolyzed Mb population, over the ~1-h time scale, is observed in glycerol/buffer mixtures at ~180 K.

To extract populations of photolyzed and ligand-bound species, we fit this region of spectrum with two major and two minor Lorentzian components. The solid lines in Figure 1 represent the four Lorentzian fit and the individual Lorentzian components. The population ratio, R_p, of bound, N_A, to the photolyzed, $1 - N_A$, species is calculated as the area ratio of the 1372- and 1356-cm^{-1} Lorentzians, corrected for the Raman cross section difference of these two modes at 425 nm ($\sigma_{1356}/\sigma_{1372} = 0.74$; Bangcharoenpaurpong et al., 1984; Morikis, 1990). The fraction of CO-bound molecules is then extracted ($N_A = R_p/(1 + R_p)$) and shown in Figures 2 and 3 as a function of laser irradiation (or pumping) time. The data for aqueous buffer (Figure 2) and for 75% glycerol (Figure 3) samples are shown for a variety of temperatures. Two general features of the pumping process, a very mild temperature dependence and a power law nature, can be discerned from the figures. The vertical shift of the data with temperature reflects the temperature dependence of k_{BA} and other fast processes that may be present. A "preequilibrium" is established with time constant τ_{eq} and is not observed directly on these long time scales. The aqueous buffer and glycerol/buffer data show pumping effects that are similar in magnitude except in the 160–190 K region, where the effect in glycerol samples reaches a maximum.

A summary of the temperature dependence of the pumping process is given in Figure 4, where we present the slope of the log–log plots of $N_A(t)$ from Figures 2 and 3. Since $N_A(t)$ behaves roughly like a power law, $N_A(t) = C(t/t_0)^{-\theta}$, the time

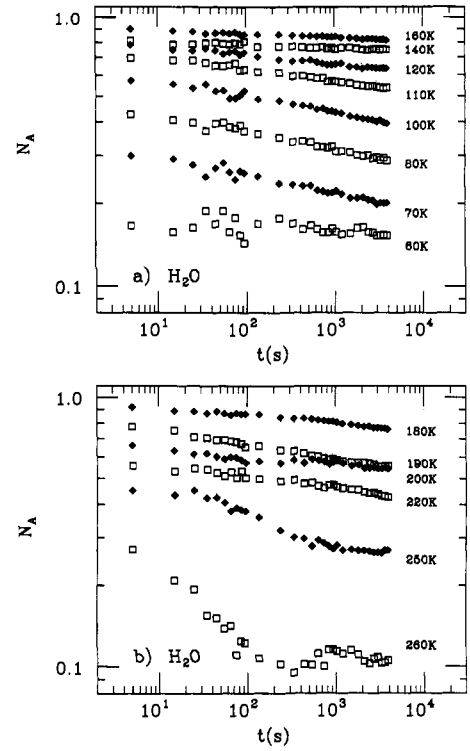

FIGURE 2: The fraction of CO-bound species, N_A, as a function of the laser illumination time, extracted from resonance Raman spectra. Data for aqueous buffer samples are presented for a variety of temperatures. A slow decrease in N_A is stretched over at least three decades in time, and the slope of the log–log plot exhibits a very weak temperature dependence below 250 K. Above 250 K, the slope is steeper as the ligands begin to escape to the solvent and equilibrium is established within the time limit of the experiment.

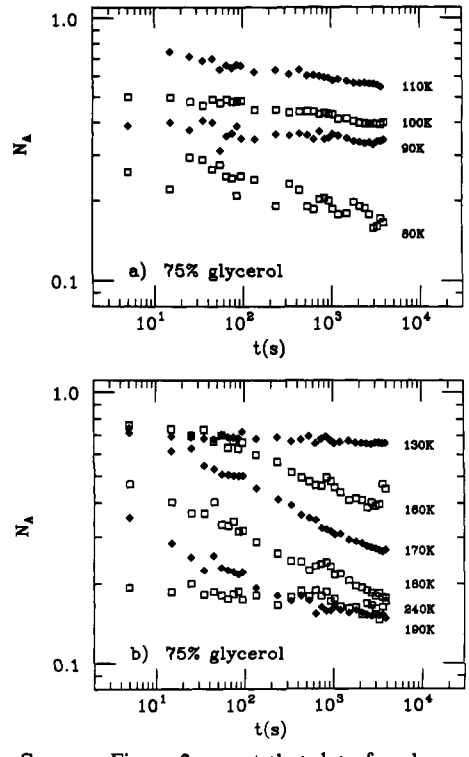

FIGURE 3: Same as Figure 2 except that data for glycerol/buffer MbCO samples are presented. It can be seen that there is a significant increase in the N_A decay rate around 180 K in glycerol samples. Above ~180 K the ligand begins to escape protein and enter the solvent.

exponent θ is the slope of the log–log plot. In the instances where the data do not have a constant slope on the log–log plots of $N_A(t)$, θ is calculated as the slope of the line joining

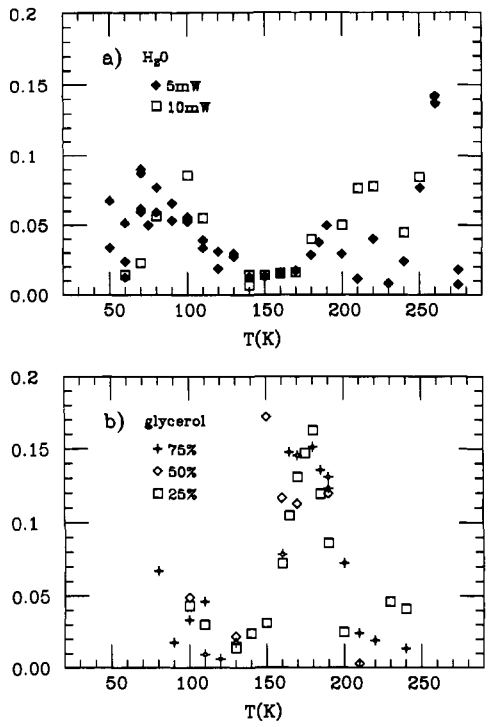

FIGURE 4: Summary of temperature dependence of the pumping process for aqueous buffer (a) and glycerol/buffer (b) samples. The slope, θ, of the log N_A versus log t plot, from Figures 2 and 3, is presented as a function of temperature. There are increases in the slopes around 250 K for aqueous samples and around 180 K for glycerol samples. These are attributed to a "melting" transition of the protein/solvent system.

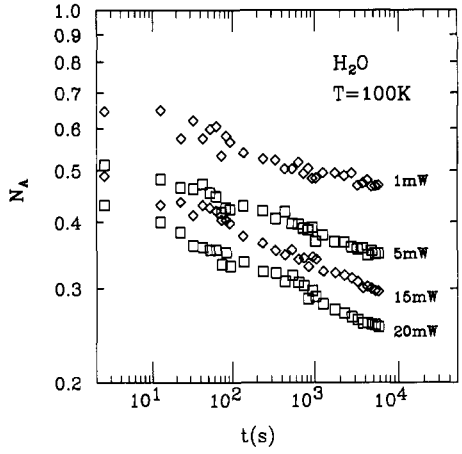

FIGURE 5: The laser power dependence of the pumping process. The time dependence of the fraction of CO-bound molecules is presented for several laser powers, for the aqueous buffer MbCO samples at 100 K. The data reveal that the pumping rate was only weakly affected by the laser powers applied to the sample.

the end points of the process and thus represents an "average" slope. Although the slopes are somewhat scattered, due to noise in the $N_A(t)$ data, it can be seen that, in glycerol samples (b), there is a significant increase in the slope around 180 K. In aqueous samples (a), this feature is absent but a small increase in slopes around 80 K and a bigger increase around 260 K can be discerned.

The laser power dependence of the pumping process is displayed in Figure 5. Here we present the decrease in CO-bound population fraction, N_A, during pumping of an aqueous sample at 100 K, for several different laser powers. These data show that, at least over the limited range of laser powers used, the rate of pumping is only weakly affected by the laser power applied. It should be pointed out that laser-induced heating

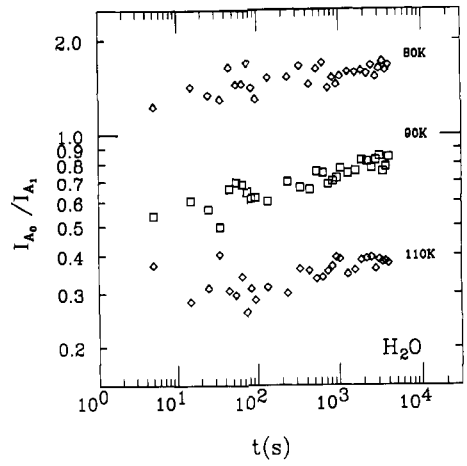

FIGURE 6: The effect of different heme pocket environments on the pumping process. The intensity ratio of 491 and 508 cm^{-1} resonance Raman Fe–CO modes is presented as a function of time, for pH 7 aqueous buffer (0.1 M KP_i) MbCO samples at low temperatures. These two modes are associated with two different pocket conformations: 491 cm^{-1} with the A_0 or open pocket conformation; 508 cm^{-1} with the A_1 or closed pocket conformation. Thus, the intensity ratio of these two modes is proportional to the relative populations of the two conformations. The increase in the I_{A_0}/I_{A_1} ratio that is observed indicates that the molecules in the A_1 conformation are pumped more efficiently.

effects are expected to increase $\langle k_{BA} \rangle$ with time and cause an increase in $N_A(t)$ rather than the observed decrease during pumping.

Finally, we have also characterized the pumping process in an aqueous pH 7 sample by monitoring the populations of two different MbCO configurations observed at low temperatures (Reinisch et al., 1987; Šrajer, 1991). They are distinguished by different Fe–CO stretching mode Raman frequencies: 510 cm^{-1} for a configuration with CO in a bent or tilted geometry (A_1) and 490 cm^{-1} for a configuration with CO in a more linear geometry (A_0) with respect to the heme normal. It is shown in Figure 6 that the intensity ratio of these two modes, I_{A_0}/I_{A_1}, is increasing during the pumping process, suggesting that the more rapidly rebinding A_0 species is pumped less effectively than the A_1 species.

To observe the rebinding from the pumped state, we have employed procedure II. The results are displayed in Figure 7, where we plot the fraction of photolyzed molecules, $1 - N_A$, as a function of time, after the pumping laser light is blocked. The solid diamonds represent the rebinding from the pumped state for several temperatures. The amplitudes (offsets) in this figure at $t = 1$ min reflect the number of molecules in the pumped state since the geminate rebinding, characterized by flash photolysis experiments, is already complete on this time scale. The fraction of photolyzed molecules, $1 - N_A$, was found by monitoring the full Soret region and fitting the band shape with $N_A S_{MbCO} + (1 - N_A) S_{Mb^*}$, where S_{MbCO} is the measured MbCO Soret spectrum at a given temperature and S_{Mb^*} is the measured Soret spectrum of the low-temperature photoproduct Mb*. (Since complete photolysis cannot be achieved at all temperatures, the Mb* spectrum at 10 K was used.)

In order to assess the hypothesis that, in the pumping process, the CO molecule escapes into the solvent matrix, we have compared the rebinding from the pumped state with the rebinding from the frozen solvent. To prepare an ensemble of photolyzed MbCO molecules with a significant amount of CO outside the protein, we cooled the MbCO sample under laser illumination (procedure III). The open diamonds in Figure 7 correspond to rebinding from the solvent by use of this procedure. The fraction of photolyzed molecules was

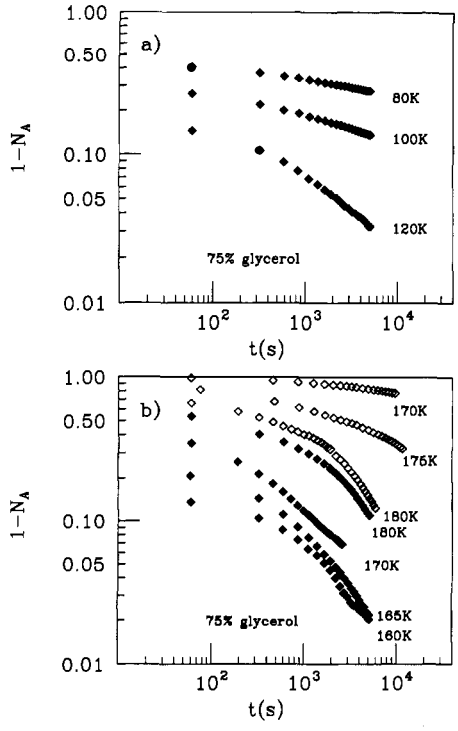

FIGURE 7: The fraction of photolyzed molecules ($1 - N_A$) as a function of time during rebinding from the pumped state presented at several temperatures for glycerol/buffer MbCO samples (◆). The observed kinetics probes only the pumped component of the population, since geminate rebinding from the unpumped states occurs on much faster time scales. In order to compare it with the rebinding from the protein exterior at similar temperatures, samples were frozen under laser illumination. These rebinding kinetics are represented by the ◇. The data show that the rebinding from the pumped state is nonexponential and, also, that the pumped state is not simply a state with the CO molecule in the exterior solvent.

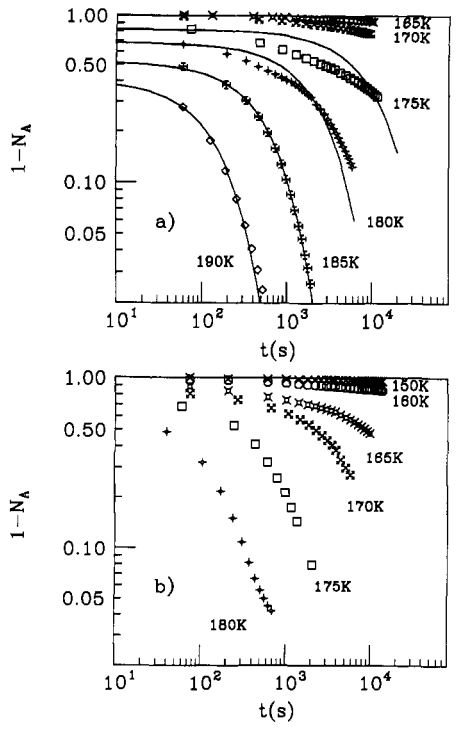

FIGURE 8: Rebinding kinetics after the MbCO sample was cooled under laser illumination. This experimental procedure allows a significant fraction of protein molecules to be frozen with the CO exterior to the protein, so that rebinding from the solvent can be monitored with a large amplitude below 200 K. In this temperature range, the observed rebinding rate is limited by the ligand entry rate k_{in}, which is directly measured. The data show that this rate is slower for more viscous 75% glycerol samples (a) than for the 50% glycerol samples (b). The solid lines in panel a represent the exponential extrapolation of the flash photolysis results (Austin et al., 1975) to $T < 200$K. A nonexponential to exponential transition around 180 K is also observed and indicates a transition of the protein/solvent system at this temperature.

extracted from fits of the Soret region in the same way as for rebinding from the pumped state, described above. The data show that, below 180 K, the pumped state and the state with the CO molecule in the solvent (or protein exterior) are two distinct states with different rebinding properties. Above 180 K, however, the two states cannot be distinguished since they have the same rebinding rate, indicating that above 180 K the CO molecule does leave the heme pocket during extended photolysis and rebinds from the exterior of the protein.

In Figure 8, we present more detailed rebinding data obtained after the sample was cooled under illumination. As in Figure 7, we plot the fraction of photolyzed molecules as a function of time after the photolyzing laser light is turned off. The rebinding rate for a given temperature is a function of solvent composition (75% glycerol data shown in (a), 50% glycerol data shown in (b)) and the CO concentration (not shown), as expected for rebinding from the solvent. Rebinding is faster for the less viscous 50% glycerol/buffer samples. Rebinding from the solvent was measured previously in flash photolysis experiments at temperatures above 210 K (process IV in Austin et al. (1975)) but not for lower temperatures because of its diminishing amplitude. Note that below 220 K the observed rebinding rate (λ_{IV} in Austin et al. (1975)) is equal to the rate of CO moving from the solvent to the pocket (Austin et al., 1975), k_{in}, so that the ligand entry rate is measured directly at these temperatures. These are the first measurements of the entry rate at temperatures below 200 K, where the amplitude of the entry process has been greatly enhanced by freezing the sample under CW laser illumination. A similar effect, with much smaller amplitude, has also been noted by Berendzen and Braunstein (1990) using a temperature derivative spectroscopy. Extrapolations of flash photolysis measurements (Austin et al., 1975) to lower temperatures are given as the solid lines in Figure 8a (to generate these curves we used the enthalpy barrier $H_{in} \equiv H_{ed} = 79$ kJ/mol for the E → D transition from Table I of Austin et al. (1975) and a prefactor of $k_0 = 10^{19.5}$ s^{-1}, which accounts for the somewhat higher CO pressure in our experiment, [CO] = 0.5 mM, than in Austin et al.). Our data are in good agreement with the predicted exponential behavior above 180 K. Below 180 K, however, rebinding from the solvent becomes nonexponential. The variation of offset with temperature in this experiment indicates that faster processes with nonvanishing amplitude are present. Data on shorter time scales are needed to describe fully the rebinding under the experimental protocol of procedure III.

Discussion and Analysis

We first discuss pumping in the temperature region below 180 K, where only geminate rebinding is present, and compare two possible models: heme relaxation and multiple states. Within the multiple-state model we briefly address the results of extended photolysis in the region above 180 K, which is more complicated due to the escape of the CO molecule to the solvent. We also present a simple distributed barrier analysis in order to illustrate the magnitude of the distributions needed to account for the pumping process. Finally, we note that photostationary state populations of N_A vs temperature, prior to pumping, suggest solvent dependence in the rebinding barrier distribution, $g(H_{BA})$.

Heme Relaxation Hypothesis

The simplest model that can account for the observed pumping effect at temperatures below 180 K involves only two states

$$A \underset{\{k_{BA}\}}{\overset{k_1}{\rightleftharpoons}} B \qquad (1)$$

where A is a CO-bound state and B is a state without a bond between the CO molecule and the heme. The $\{k_{BA}\}$ are the distributed geminate rebinding rates ($k_{BA} = k_0 e^{-H_{BA}/k_B T}$, where k_0 is a prefactor containing an entropy barrier, H_{BA} is the enthalpy barrier, k_B is the Boltzmann constant, and T is the temperature). This model is consistent with the observations in flash photolysis experiments (Austin et al., 1975) that below 180 K only a single geminate state with distributed enthalpy barriers, H_{BA}, is needed to explain the rebinding data.

In order to incorporate the observation of the pumping effect, the distribution of enthalpy barriers, $g(H_{BA})$, needs to be allowed to evolve slowly toward higher enthalpy during the irradiation time. This evolution of the barriers can be caused by a slow relaxation of the nonequilibrium protein conformation after multiple CO photolysis events. Above ~180 K, it has been suggested (Agmon & Hopfield, 1983; Steinbach et al., 1991) that thermally induced relaxation processes lead to the diffusion of a generalized protein coordinate and to an increased barrier height at the heme. We have postulated in earlier work (Šrajer et al., 1988) that a key coordinate determining the geminate rebinding barrier involves the iron–porphyrin out-of-plane displacement, a, of the photolyzed Mb. We have also demonstrated the need to separate explicitly this (heme) coordinate from the generalized (protein) coordinate in order to allow for partial relaxation of the heme below 180 K, subsequent to photolysis. Such heme relaxation is not accounted for in the previous theoretical treatments (Agmon & Hopfield, 1983; Young & Bowne, 1984), since they lack an explicit heme coordinate and do not allow the generalized protein coordinate to relax below 180 K.

We have shown that (for a Morse potential in the iron–CO coordinate and a harmonic approximation for the iron–porphyrin displacement) the barrier for binding at the heme can be written as

$$H_{BA}(a) = \frac{1}{2}Ka^2 + H_D \qquad (2)$$

The first term in eq 2 involves the work needed to bring the heme from an unbound out-of-plane geometry to a bound in-plane geometry. The second term involves contributions to the barrier from a variety of effects including interactions between the CO and the distal pocket. The quasicontinuous distribution of rebinding barriers $g(H_{BA})$ at low temperatures, which leads to nonexponential rebinding, arises primarily from a distribution of the out-of-plane displacements, $p(a)$. The distribution, $p(a)$, has its origin in the slightly different protein conformational substates that are frozen out at low temperatures. Its explicit form is likely to be Gaussian (to lowest order in the mixing of the protein and heme coordinates), which leads to the non-Gaussian barrier height distribution, $g(H_{BA})$, given by eq 10 of Šrajer et al. (1988). Within this model, the simplest picture of protein relaxation induced by CW laser photolysis involves the evolution of the mean out-of-plane displacement, a_0^*, from its partially relaxed low-temperature photoproduct value ($a_0^* \simeq 0.2$–0.35 Å) toward a completely relaxed deoxy value (0.45 Å) through the proximal histidine link. This will increase the barriers for rebinding according to eq 2 and lead to a slower rebinding kinetics and a slow decrease in $N_A(t)$.

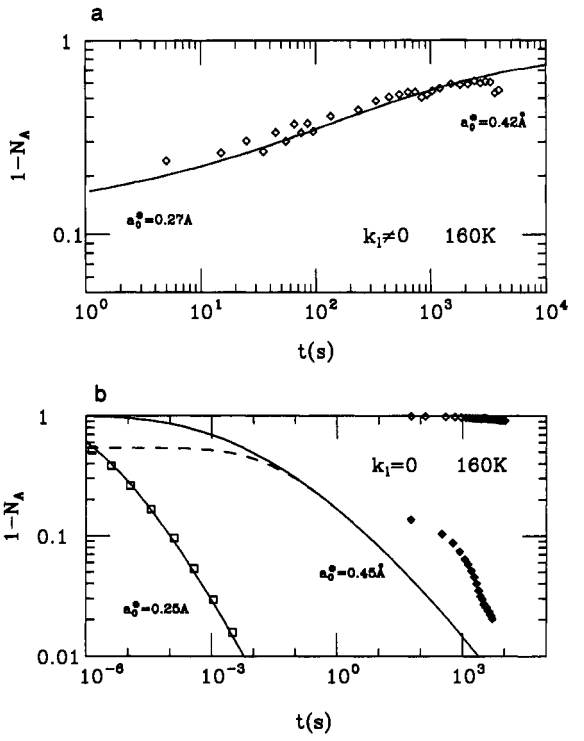

FIGURE 9: Illustration that heme relaxation subsequent to multiple photolysis events can account for the pumping process (a) but that (even with an extreme geometry change at the heme) the predicted rebinding kinetic does not slow down enough to account for the measured rebinding from the pumped state (b). The diamonds in (a) represent the increase in the fraction of photolyzed MbCO molecules during pumping, for a 75% glycerol sample at 160 K. The solid line is calculated by use of eq 3 and the assumption that photon-mediated protein relaxation leads to a "stretched" relaxation of the mean iron out-of-plane displacement: $a_0^* = 0.45\ \text{Å} - \delta_a e^{-(\gamma t)^\beta}$. The parameters used to generate the solid line are $k_1 = 5.0 \times 10^4\ s^{-1}$, $k_0 = 2.8 \times 10^9\ s^{-1}$, $T = 160$ K, $\delta_a = 0.2$ Å, $\gamma = 0.0008\ s^{-1}$, and $\beta = 0.3$. To calculate the enthalpy distribution, $g(H_{BA},t)$, eq 10 from Šrajer et al. (1988) was used with $K = 161.8$ kJ/(mol·Å^2), $\sigma_a = 0.08$ Å, and $H_D = 7$ kJ/mol. The proposed relaxation mechanism fails to predict the correct rebinding kinetics as shown in part b. The geminate rebinding B → A data (from flash photolysis) is represented by □, the rebinding after pumping for ~1 h by ◆, and, for completeness, rebinding from the protein exterior by ◇. The relaxation of a_0^*, from 0.25 to 0.45 Å, due to pumping, slows down the rebinding as shown. The solid lines simulate the flash photolysis experiment, and the dashed line utilizes eq 4 to account for the much smaller $k_1(t_p)$ in the present experiments.

In Figure 9a we illustrate that allowing a_0^* to evolve with time can account for the pumping effect. Here we plot the fraction of unbound molecules, $1 - N_A$, as a function of laser irradiation time.[1] The diamonds represent data for 160 K in 75% glycerol and the solid line is a result of the calculation

$$1 - N_A = \int \frac{k_1}{k_1 + k_{BA}(H_{BA})} g(H_{BA},t)\,dH_{BA} \qquad (3)$$

where we have assumed that $g(H_{BA},t)$ is a slowly varying function compared with the "equilibration" time $\tau_{eq} = 1/(k_1 + k_{BA})$. The evolution of $g(H_{BA},t)$ is assumed to arise from a slow increase of a_0^* with time: $a_0^* = 0.45\ \text{Å} - \delta_a \Phi(t)$, with a relaxation function, Φ, given by $\Phi(t) = e^{-(\gamma t)^\beta}$. The parameters used to generate the solid curve correspond to a change in a_0^* from 0.25 Å at $t = 0$ to 0.42 Å at $t \sim 10^4$ s and are given

[1] In the simulations shown in Figure 9 we have assumed that the laser flux can be taken as a constant. However, the attenuation and Gaussian beam density, which make k_1 a function of spatial coordinates, have also been considered in some detail (Šrajer, 1991). Simulations that allow for realistic distributions in k_1 do not significantly affect the results, so only the simpler model calculations are presented here.

in the figure caption. The initial value for a_0^* is taken to be 0.25 Å in an attempt to accommodate the large change in time scale associated with rebinding from the pumped states (see below).

Although a stretched exponential relaxation of a_0^* can account for the pumping process, it has difficulty explaining the large reduction in the rebinding rate after the pumping light is blocked, as shown in Figure 9b. In the left part of this figure we present the geminate rebinding data for MbCO at 160 K (Austin et al., 1975) as open squares and the prediction of the model (Šrajer et al., 1988), described by eq 2, as solid lines. The line going through the data points corresponds to a partially relaxed heme with $a_0^* = 0.25$ Å, while the other solid line corresponds to the reduced rebinding rate, predicted for a flash photolysis experiment, after a_0^* has fully relaxed to 0.45 Å. It should be noted that the flash photolysis data do not uniquely specify a_0^* (see Šrajer et al. (1988) for details). However, a smaller value of a_0^* (e.g., 0.25 Å) and, thus, a larger relaxation (0.25–0.45 Å) is needed to better account for the enormous increase in the rebinding time scales of the pumped states. The measured CO rebinding kinetics after ~1 h of pumping are presented by the solid diamonds on the right side of the figure. This rebinding can be described by

$$1 - N_A = \int \frac{k_1(t_p)}{k_1(t_p) + k_{BA}(H_{BA})} e^{-k_{BA}(H_{BA})(t-t_p)} g(H_{BA},t_p) dH_{BA} \quad (4)$$

where t_p denotes the instant the laser light is switched off. The dashed line in Figure 9b is predicted by this equation if a_0^* is taken to be 0.45 Å at t_p. Here we have assumed that the relaxation in the coordinate space is uniform across the ensemble (δ_q constant) and that the relaxation ceases when the pumping laser is turned off at t_p. The flash photolysis experiment is recovered in the limit $k_1(t_p) \gg k_{BA}(H)$, for all H, and leads to the solid lines in Figure 9b. Note that the observed rebinding is still an order of magnitude slower than the prediction obtained from the 0.25 ⇄ 0.45-Å relaxation of a_0^*. This suggests that an even larger, photolysis-driven heme relaxation is required to explain the pumping phenomenon.

However, a strong argument against extreme photolysis-driven heme relaxation comes from a detailed study of the Soret band line shape and position, subsequent to extended photolysis of MbCO samples (in 75% glycerol) under a variety of conditions. For example, the Mb* Soret band is observed to blue shift by ~140 cm^{-1} as the heme relaxes at temperatures above 185 K. Further experiments show only very small shifts in the optical line shapes of Mb* after pumping at temperatures below 180 K, a result inconsistent with a significant heme relaxation. This suggests that some additional mechanism must be associated with pumping below 180 K. Above 185 K, Soret band line shifts are observed, indicating that in this higher temperature region both heme relaxation and ligand escape from the pocket are occurring. The shift of the Soret band at 185 K can be considered as some of the first direct evidence for protein-induced heme relaxation at the glass transition temperature of the solvent (Šrajer & Champion, 1991; Šrajer, 1991; Champion, 1990).

Multiple-State Hypothesis

Since the low-temperature heme relaxation of a_0^* cannot account for both the extremely slow rebinding and the nearly unaltered optical properties observed after pumping the sample below 180 K, we propose the modification of eq 1 to include an additional geminate state, C, with a much smaller CO rebinding rate than state B. We expect that state C is a state with the CO still in the heme pocket or a cavity near the pocket, since the rebinding from the solvent (procedure III) at these temperatures (open diamonds, Figure 9b) is even slower than rebinding from the pumped state (solid diamonds). Thus, Figure 9b shows three very different rebinding rates at 160 K and illustrates the presence of three distinct states of photolyzed MbCO at low temperatures.

There are at least two possible assignments for the geminate states B and C. In the first, state B corresponds to a "contact pair" state and state C to a "separated geminate pair" with the CO in a position farther from the iron (perhaps within a crevice of the heme cavity). A third photolyzed state, S, corresponds to the CO at the exterior of the protein or in the solvent. In making these assignments, we recall that two distinct geminate rebinding processes in Mb have been observed in room temperature rebinding kinetics measurements (Jongeward et al., 1988), for all ligands (O_2, NO, isocyanides) except CO. The faster, picosecond process is attributed (Jongeward et al., 1988) to a "contact geminate pair" recombination with a ligand that has experienced just a slight translational and rotational motion compared to its bound position and orientation. At room temperature, the contact pair recombination is not observed in MbCO, presumably due to a vanishing amplitude associated with the fast migration of the ligand into the distal pocket. At low temperatures, however, this process is greatly slowed down and the contact pair recombination will dominate the rebinding kinetics if the escape from the contact pair state is blocked by the "frozen" protein residues. The room temperature nanosecond process is attributed to the "separated geminate pair" where the ligand has rotated and moved to a more distant location within the pocket (Carver et al., 1990). The rebinding from this state can only be observed with ca. 4% amplitude (Henry et al., 1983) for MbCO at room temperature, due to the rapid rate of CO escape from the pocket to the solvent.

A second interpretation of the states is that state B corresponds to a CO molecule in the heme pocket and state C to a CO molecule being "trapped" in another cavity while migrating through the protein matrix. Several cavities are known to exist and are sampled by the CO molecules on their way to the solvent in molecular dynamics simulations (Elber & Karplus, 1990). The most common CO trajectory, in the rigid protein simulations that mimic the low-temperature conditions, is found to explore the AB/G cavity. Thus, the laser-induced pumping process can be interpreted as experimental evidence for this type of CO trajectory. Our limited study of heme-octapeptide at 10 K supports the idea that the pumped state is a state with the CO molecule trapped in a cavity of the protein, since we observe only a very small pumping effect in this sample. However, these experiments cannot distinguish between the heme cavity (or pocket) and other, more distant, cavities in the protein matrix.

As a result of the discussion above, we find that, in order to be consistent with the CW laser induced pumping experiments of MbCO at low temperature, a minimal set of four sequential states is needed.

$$A \underset{k_{BA}}{\overset{k_1}{\rightleftharpoons}} B \underset{k_{CB}}{\overset{k_{BC}}{\rightleftharpoons}} C \underset{k_{in}}{\overset{k_{out}}{\rightleftharpoons}} S \quad (5)$$

The A, B, and C states are described above. These three states are needed to account for the experiments at temperatures below 180 K, involving flash photolysis and procedure II, since two geminate rebinding processes are observed. The fourth state, S, corresponding to the CO molecule at the protein exterior or in the solvent, is needed to account for the ultraslow rebinding population observed after freezing of the sample under laser light illumination (procedure III). All three of

these rebinding processes are shown in Figure 9b (rebinding from C and S is shown in more detail in Figures 7 and 8).

As shown in Figure 7b for glycerol/buffer samples, the ligand rebinding from the solvent (procedure III) and from the pumped state (procedure II) cannot be discriminated as the temperature approaches 185 K. For this reason, we mark this temperature as a "melting" temperature of the protein/solvent system and attribute the big increase in the slope of the log N_A vs log t plots around 180 K (Figure 4b) to the increased k_{out} rate, not simply to an increase in the rate k_{BC}. In aqueous samples, the rapid increase in the slope is shifted to ~260 K. Due to the opaque nature of the frozen aqueous samples, a more direct measurement (rebinding kinetics) of the temperature at which CO escapes into the aqueous solvent could not be made. The slope falls off again when the temperature is increased beyond the melting transition (note the resonant features in Figure 4, parts a and b, at 260 K and 180 K). This is probably due to a further increase in k_{BC} and k_{out} that results in rapid equilibration prior to the monitored time window. The resonant features of the plots in Figure 4 can thus be used to determine the temperature where thermally induced conformational fluctuations allow the ligand to escape into the solvent. We find that this temperature is ~180 K for glycerol/buffer samples and ~260 K for aqueous buffer samples. These values agree with the protein phase transition temperatures observed in various other experiments for both glycerol/buffer and aqueous buffer samples (Caughey et al., 1981; Parak et al., 1984; Ansari et al., 1987; Reinisch et al., 1987; Iben et al., 1989; Doster et al., 1990; Morikis, 1990). They also agree with the observation (Iben et al., 1989) that the protein phase transition is "slaved" to a solvent phase (or glass) transition.

In either the two-state heme relaxation model or the three-state model for pumping, it is expected that the time spent in the unbound configuration, $t_{off} = [k_l/(k_l + k_{BA}(H))]t$, affects the pumping efficiency. Clearly, the heme can not relax and the ligand can not escape to C when the system is in the bound state. This suggests that proteins with large values of k_{BA} are the least likely to be pumped.

Flash photolysis experiments (Ansari et al., 1987) are in accord with this view and show that fast rebinding species are basically unaffected by pumping, while the slowly rebinding species get pumped into even slower rebinding states. The data from Figure 6 also show that the pumping process is sensitive to the heme pocket environment and is less effective for the faster rebinding A_0 state. This state has been associated (Morikis et al., 1989) with the "open" conformation where distal histidine swings out of the heme pocket toward the solvent (Kuriyan et al., 1986). The alteration of the distal structure and reduced CO steric hindrance in the open form may, thus, reduce the likelihood of leaving the "contact pair" state or the heme pocket.

In order to deduce if the transition from state B to state C is photon assisted (i.e., if k_{BC} depends explicitly upon k_l), we again recall the results of the pumping experiment at different laser powers, shown in Figure 5. They indicate that the B → C process is not photon induced, since only a small increase in pumping rate is observed when the laser power is increased. Because the overall rate of escape is given by $k_l k_{BC}/(k_l + k_{BA})$, we would expect to observe a strong (at least quadratic) dependence of the pumping rate on laser flux if k_{BC} were photon driven.

Distributed Barrier Analysis

Finally, we want to address the issue of the stretched, power law behavior of the pumping process and subsequent rebinding from the pumped state. There are a variety of possible models that can be used to account for the spread of the pumping process over many orders of magnitude in time (e.g., parallel B → C channels within each protein, uniformly random distributions of the fastest channel, etc.). However, for simplicity, we have chosen to invoke a distribution of rates k_{BC} and k_{CB}, similar to the approach that was taken (Austin et al., 1975; Šrajer et al., 1988) to account for the power law nature of the geminate rebinding B → A.

In order to reproduce the observed spread in time over a wide range of temperatures, very broad distributions are needed. In Figure 10 we illustrate the effect of distributing the barriers associated with k_{BC} and k_{CB}. The rates k_{BC} and k_{CB} are assumed to be of the Arrhenius form $k = k_0 e^{-H/k_B T}$. In part a of the figure we have correlated the enthalpies H_{BC} and H_{CB} so that $H_{CB} = H_{BC} + \Delta$ and used a Gaussian distribution of H with a width σ_H. In part b we assumed $\langle H_{BC} \rangle = \langle H_{CB} \rangle = 0$ so that the rates k_{BC} and k_{CB} are of the form $k = k_0 = \nu e^{S/k_B}$. We have correlated the entropies S_{BC} and S_{CB} and used a Gaussian distribution of S with a width σ_S. It is probable that a combination of these two possibilities is taking place and that the distributions are more complicated than simple correlated Gaussians. Since the data do not carry enough information to specify uniquely the distributions associated with k_{BC} and k_{CB}, we have chosen these two simple cases to illustrate the magnitude of the effect.

The "yield" for the creation of the pumped state can be approximated by $k_{BC}(\langle H_{BC} \rangle)/[k_{BC}(\langle H_{BC} \rangle) + k_{BA}(\langle H_{BA} \rangle)]$. If one takes the data in Figure 10a as an example, the yield at 100 K is estimated to be $\sim 5.0 \times 10^{-7}$ by use of the model calculations. Since the k_{BC} rates show a very different temperature dependence than the k_{BA} rates, it must be recognized that the pumping yield is quite sensitive to temperature.

Solvent Effects on $g(H_{BA})$

The distribution $g(H_{BA})$ extracted from the flash photolysis data (Austin et al., 1975) for MbCO in 75% glycerol, with $H_{BA}^{peak} \neq \langle H_{BA} \rangle$ (see Figure 6 in Šrajer et al. (1988), for example), is found to be incompatible with the aqueous sample data presented in Figure 10. A distribution of the same shape but with H_{BA}^{peak} lowered by ~3 kJ/mol, is much more consistent with the aqueous data and is used to generate solid lines in this figure. The lower value of H_{BA}^{peak} is needed in order to account for the vertical spacing between the data in Figure 10 taken at the different temperatures. The shape of the distribution and the prefactor $k_0 = 2.2 \times 10^9\ s^{-1}$ for the k_{BA} rate are taken from Šrajer et al. (1988).

In order to investigate the possible solvent effects on $g(H_{BA})$, we display in Figure 11a the ratio $(1 - N_A)/N_A$ for pH 7 aqueous buffer MbCO samples under CW laser irradiation (5-mW laser power) as a function of $1/T$ for two time limits (open diamonds at $t = 5$ s and solid diamonds at $t = 4000$ s). Below 180 K, this ratio is calculated, neglecting pumping,[2] by using the $g(H_{BA})$ distribution with $H_{BA}^{peak} \sim 11$ kJ/mol. The calculations are shown by dashed lines for two values of k_l: $k_l = 3.0 \times 10^3\ s^{-1}$ for the upper dashed line (to match data in the higher temperature region) and $k_l = 100\ s^{-1}$ for the lower dashed line (to match data in the lower temperature region). The data do not follow the trend predicted by this distribution (note the log scale). Instead, the data are more compatible with a distribution $g(H_{BA})$ of the same shape but shifted such

[2] In calculating the solid and dashed lines in Figure 11, we neglected, for simplicity, pumping effects since the slope of $(1 - N_A)/N_A$ vs $1/T$ not significantly altered during the pumping process, as can be seen from the figure.

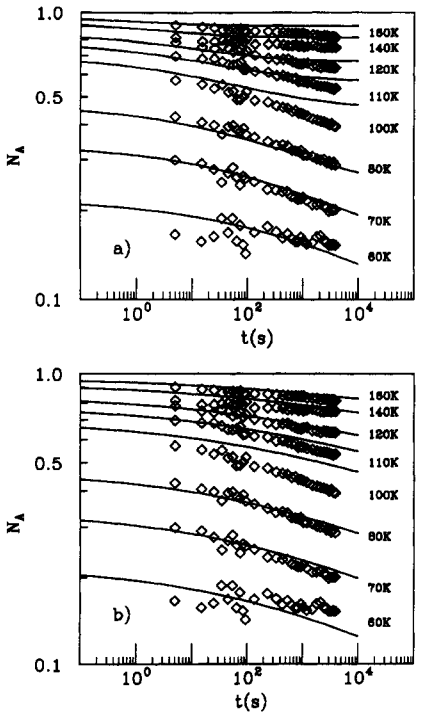

FIGURE 10: An attempt to account for the stretched, power law nature and weak temperature dependence of the pumping process. We plot the CO-bound fraction of the molecules as a function of time. The solid lines are the results of a kinetics calculation for the three-serial-state model (eq 5). A distribution for the enthalpy barrier H_{BA} from flash photolysis data in 75% glycerol samples (Šrajer et al., 1988) was shifted for ~3 kJ/mol in order to account for the vertical offsets of the displayed data. Additional distributed enthalpy barriers H_{BC} and H_{CB} are applied to generate the solid lines in (a). The barriers H_{BC} and H_{CB} are correlated so that $H_{CB} = H_{BC} + \Delta$. In the same fashion, we have distributed and correlated the entropy barriers S_{BC} and S_{CB}, to give the fits shown in (b) as solid lines. The parameters used in the calculation of solid lines are (a) $\langle H_{BC} \rangle = 6$ kJ/mol, $\Delta = 2$ kJ/mol, $\sigma_{H_{BC}} = 3$ kJ/mol, $k_0 = 100$ s^{-1} for both rates k_{BC} and k_{CB}, and $k_l = 7.0 \times 10^3$ s^{-1}; (b) $S_{BC}/k_B = -37$, $\Delta/k_B = -4.5$, $\sigma_{S_{BC}/k_B} = 7$, $\upsilon = 10^{13}$ s^{-1} for both rates k_{BC} and k_{CB}, and $k_l = 7.0 \times 10^3$ s^{-1}.

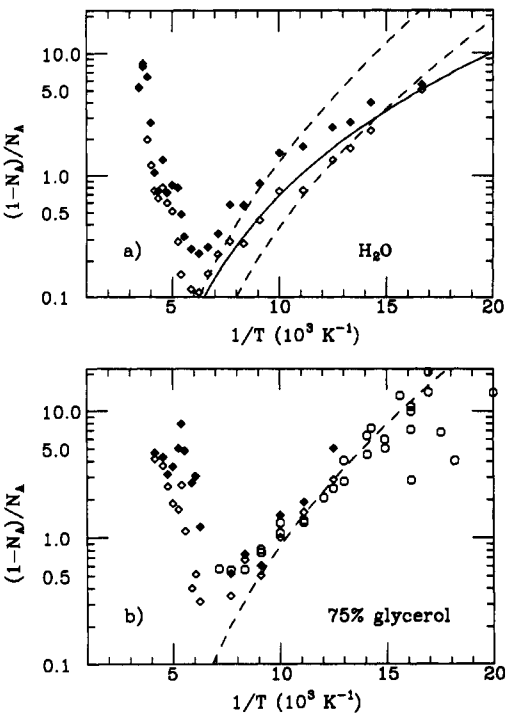

FIGURE 11: The ratio of deoxy/bound material as a function of $1/T$ obtained from the Raman intensities of MbCO in aqueous (a) and 75% glycerol (b) solvents. ◇ represent the ratios at $t = 5$ s and ◆ correspond to $t = 4000$ s during the pumping experiment. ○ in panel b represent early time data ($t = 60$ s) from additional runs that extend to lower temperatures. Some of the low-temperature data points in (b) are scattered, reflecting the difficulty in determining the ratio at low temperatures in a glycerol matrix (e.g., high fluorescence background, variations in k_l, and penetration depth due to the cracks in the sample, etc.). The dashed lines and solid line are calculations of the steady-state ratio as a function of the peak in the $g(H_{BA})$ distribution: $H_{BA}^{peak} \sim 11$ kJ/mol (dashed) and $H_{BA}^{peak} \sim 8$ kJ/mol (solid). The shape of the distribution and a prefactor $k_0 = 2.2 \times 10^9$ s^{-1} for k_{BA} rate are taken from Šrajer et al. (1988). In (a), we illustrate that an alteration of the laser photolysis rate from $k_l = 3 \times 10^3$ s^{-1} (upper dashed curve) to 10^2 s^{-1} (lower dashed curve) only shifts the curves on the logarithmic scale and does not alter their slopes. The solid line in (a) that follows the trend of the data for aqueous samples better than the dashed lines is calculated with the shifted distribution ($H_{BA}^{peak} \sim 8$ kJ/mol) and $k_l = 2 \times 10^4$ s^{-1}. On the other hand, the dashed line in (b), generated with $H_{BA}^{peak} \sim 11$ kJ/mol distribution and $k_l = 10^3$ s^{-1}, is more consistent with the 75% glycerol data.

that $H_{BA}^{peak} \sim 8$ kJ/mol (solid line). A much more reasonable value of $k_l = 2.0 \times 10^4$ s^{-1} is also found by use of the shifted distribution. Similar data taken with the low pH aqueous buffer samples (pH 5.8; not shown) exhibit an even bigger discrepancy with the results of flash photolysis experiments using glycerol samples (Doster et al., 1982). The required H_{BA}^{peak} in the low pH aqueous samples is ~3 kJ/mol compared with ~8 kJ/mol obtained from the flash photolysis experiments in 75% glycerol at low pH.

A significant solvent dependence of the $g(H_{BA})$ distribution is further indicated by the data for 75% glycerol samples in Figure 11b. These data show much better agreement with the $H_{BA}^{peak} \sim 11$ kJ/mol distribution obtained from flash photolysis experiments with 75% glycerol samples (dashed line, $k_l = 10^3$ s^{-1}). The present results do not agree with the conclusions of Beece et al. (1980) that the barrier distribution for the step B → A is solvent independent below 200 K. One obvious explanation is that the ratio of "open" and "closed" states is affected by the solvent and its freezing temperature. It has been shown (Ansari et al., 1987) that the relative population of faster rebinding A_0 species is significantly larger in the frozen aqueous samples than in 75% glycerol samples. If the A_0 state has a lower rebinding barrier, its larger population in the frozen aqueous samples could account for the solvent differences noted in Figure 11. However, this explanation is not in accord with the suggestion of Ansari et al. (1987) and Braunstein et al. (1988) that the increased rebinding rate of the A_0 state is due to an entropy effect. Another possibility is that $a_0^*(H_2O) < a_0^*(\text{glycerol})$.

SUMMARY

We have used a new CW laser protocol to study the effects of extended photolysis of MbCO at low temperatures. We find that a significant population of photolyzed geminate states with increased lifetime is created (i.e., the laser pumps the molecules into long-lived states). A simple two-state model with a slow, photolysis-induced heme relaxation that increases the barriers for rebinding can explain the time-dependent evolution of the pumping phenomenon. However, this explanation is not in good quantitative agreement with the extremely slow rebinding process observed after the pumping laser light is blocked, unless very large alterations in the heme geometry are taking place. Such large alterations in geometry should lead to measurable changes in the optical line shapes and positions. Since no significant optical changes due to pumping are observed below 180 K (Šrajer & Champion, 1991), we introduce an additional (sequential) geminate state, C, into the low-temperature analysis. This state (or states) may be analogous to the "separated geminate pair" observed in the room temperature kinetics (Jongeward et al., 1988;

Henry et al., 1983). The state C can also be interpreted as a CO molecule trapped in a cavity on its way through the protein matrix. Since the pumping process and the rebinding from the pumped state exhibit a power law behavior and a very weak temperature dependence, broad distributions in enthalpy and/or entropy for the transitions between B and C are used to account for the data. These distributions presumably arise from different protein conformational states that are trapped as the system is frozen (quenched disorder). A variety of other models, describing parallel pathways for the ligand migration from B to C, also lead to the observed power law behavior but have difficulty accounting simultaneously for the rebinding reaction.

Below 180 K only geminate states are present, for samples frozen in the dark, but at ~180 K in glycerol/water samples we have observed the "melting" of the protein. This allows the CO molecule to escape into the solvent during extended laser photolysis. The transition temperature for aqueous samples is ~260 K. Both of these temperatures are consistent with a protein transition that is slaved to a solvent phase (or glass) transition.

In an experimental protocol where the sample is cooled under laser illumination (procedure III), we have succeeded in maintaining a significant fraction of the Mb molecules in a state with the CO at the exterior of the protein. This enables us to measure the rebinding of CO from the solvent at temperatures below 200 K for the first time with such large amplitudes. The rebinding kinetics from the solvent also suggest a rather sharp protein phase transition at ~180 K, since an exponential to nonexponential transition in rebinding is observed in this temperature region. Between 180 and 200 K the exponential rebinding observed with the new protocol is in good agreement with the parameters used to describe the solvent process at higher temperatures (Austin et al., 1975). The transition in the kinetics at ~180 K is consistent with recent studies of the optical properties of photolyzed MbCO. In these studies a sharp transition at 185 K, involving structural relaxation of the heme chromophore, is observed by monitoring a ~140-cm^{-1} shift of the Soret band (Šrajer & Champion, 1991).

Acknowledgments

We thank Prof. Robert Markiewicz for stimulating discussions.

Registry No. CO, 630-08-0; heme, 14875-96-8; glycerol, 56-81-5.

References

Agmon, N., & Hopfield, J. J. (1983) *J. Chem. Phys. 79*, 2042.

Ansari, A., Berendzen, J. B., Braunstein, D., Cowen, B. R., Frauenfelder, H., Hong, M. K., Iben, I. E. J., Johnson, J. B., Ormos, P., Sauke, T. B., Scholl, R., Schulte, A., Steinbach, P. J., Vittitow, J., & Young, R. D. (1987) *Biophys. Chem. 26*, 337.

Austin, R. H., Beeson, K. W., Eisenstein, L., Frauenfelder, H., & Gunsalus, I. C. (1975) *Biochemistry 14*, 5355.

Bangcharoenpaurpong, O., Schomacker, K. T., & Champion, P. M. (1984) *J. Am. Chem. Soc. 106*, 5688.

Beece, D., Eisenstein, L., Frauenfelder, H., Good, D., Marden, M. C., Reinisch, L., Reynolds, A. H., Sorensen, L. B., & Yue, K. T. (1980) *Biochemistry 19*, 5147.

Berendzen, J., & Braunstein, D. (1990) *Proc. Natl. Acad. Sci. U.S.A. 87*, 1.

Braunstein, D., Ansari, A., Berendzen, J., Cowen, B. R., Egeberg, K. D., Frauenfelder, H., Hong, M. K., Ormos, P., Sauke, T. B., Scholl, R., Schulte, A., Sligar, S. G., Springer, B. A., Steinbach, P. J., & Young, R. D. (1988) *Proc. Natl. Acad. Sci. U.S.A. 85*, 8497.

Carver, T. E., Rohlfs, R. J., Olson, J. S., Gibson, Q. H., Blackmore, R. S., Springer, B. A., & Sligar, S. G. (1990) *J. Biol. Chem. 265*, 20007.

Case, D. A., & Karplus, M. (1979) *J. Mol. Biol. 132*, 343.

Caughey, W. S., Shimada, H., Choc, M. G., & Tucker, M. P. (1981) *Proc. Natl. Acad. Sci. U.S.A. 78*, 2903.

Champion, P. M. (1990) in *Proceedings of the Conference on The Dynamics and Kinetics of the Myoglobin and Hemoglobin* (Brunori, M., Eaton, W. A., Gibson, Q. H., & Karplus, M., Eds.) NIH, Bethesda, MD.

Champion, P. M., & Sievers, A. J. (1980) *J. Chem. Phys. 72*, 1569.

Chance, B., Powers, L., Zhou, Y.-H., & Naqui, A. (1986) *Bull. Am. Phys. Soc. 31*, 386.

Doster, W., Beece, D., Bowne, S. F., Di Iorio, E. E., Eisenstein, L., Frauenfelder, H., Reinisch, L., Shyamsunder, E., Winterhalter, K. H., & Yue, K. T. (1982) *Biochemistry 21*, 4831.

Doster, R., Cusack, S., & Petry, W. (1990) *Phys. Rev. Lett. 65*, 1080.

Elber, R. & Karplus, M. (1990) *J. Am. Chem. Soc. 112*, 9161.

Frauenfelder, H., Petsko, G. A., & Tsernoglou, D. (1979) *Nature (London) 280*, 558.

Hartmann, H., Parak, F., Steigemann, W., Petsko, G. A., Ringe Ponzi, D., & Frauenfelder, H. (1982) *Proc. Natl. Acad. Sci. U.S.A. 79*, 4967.

Henry, E. R., Sommer, J. H., Hofrichter, J., & Eaton, W. A. (1983) *J. Mol. Biol. 166*, 443.

Iben, I. E. T., Braunstein, D., Doster, W., Frauenfelder, H., Hong, M. K., Johnson, J. B., Luck, S., Ormos, P., Schulte, A., Steinbach, P. J., Xie, A. H., & Young, R. D. (1989) *Phys. Rev. Lett. 62*, 1916.

Jongeward, K. A., Magde, D., Taube, D. J., Marsters, J. C., Traylor, T. G., & Sharma, V. S. (1988) *J. Am. Chem. Soc. 110*, 380.

Kottalam, J., & Case, D. A. (1988) *J. Am. Chem. Soc. 110*, 7690.

Kuriyan, J., Wilz, S., Karplus, M., & Petsko, G. A. (1986) *J. Mol. Biol. 192*, 133.

Morikis, D. (1990) Ph.D. Dissertation, Northeastern University, Boston, MA.

Morikis, D., Champion, P. M., Springer, B. A., & Sligar, S. G. (1989) *Biochemistry 28*, 4791.

Parak, F., & Knapp, E. W. (1984) *Proc. Natl. Acad. Sci. U.S.A. 81*, 7088.

Parak, F., Knapp, E. W., & Kucheida, D. (1982) *J. Mol. Biol. 161*, 177.

Powers, L., Sessler, J. L., Woolery, G. L., & Chance, B. (1984) *Biochemistry 23*, 5519.

Reinisch, L., Šrajer, V., & Champion, P. M. (1987) *Bull. Am. Phys. Soc. 33*, 1412.

Šrajer, V. (1991) Ph.D. Dissertation, Northeastern University, Boston, MA.

Šrajer, V., & Champion, P. M. (1991) *Biochemistry* (submitted for publication).

Šrajer, V., Reinisch, L., & Champion, P. M. (1988) *J. Am. Chem. Soc. 110*, 6656.

Steinbach, P. J., Ansari, A., Berendzen, J., Braunstein, D., Chu, K., Cowen, B. R., Ehrenstein, D., Frauenfelder, H., Johnson, J. B., Lamb, D. C., Luck, S., Mourant, J. R., Nienhaus, G. U., Ormos, P., Philipp, R., Scholl, R., Xie, A., & Young, R. D. (1991) *Biochemistry* (in press).

Young, R. D., & Bowne, S. F. (1984) *J. Chem. Phys. 81*, 3730.